Journal of Molecular Liquids 426 (2025) 127305

Contents lists available at ScienceDirect

Journal of Molecular Liquids

journal homepage: www.elsevier.com/locate/molliq

Adsorption of methylene blue from aqueous solution using chitosan polymer-impregnated Tricholoma matsutake fungal biomass

Anjani R.K. Gollakota [a,*], Munagapati Venkata Subbaiah [b], Arshdeep Singh [c], Chi-Min Shu [d,*], Prakash Kumar Sarangi [e], Jet-Chau Wen [b,d]

[a] Department of Chemical and Materials Engineering, National Yunlin University of Science and Technology, Douliu City, Yunlin County 64002, Taiwan, ROC
[b] Research Centre for Soil & Water Resources and Natural Disaster Prevention (SWAN), National Yunlin University of Science and Technology, Douliu City, Yunlin County 64002, Taiwan, ROC
[c] Department of Chemistry, National Cheng Kung University, Tainan, Taiwan
[d] Department of Safety, Health and Environmental Engineering, National Yunlin University of Science and Technology, Douliu City, Yunlin County 64002, Taiwan, ROC
[e] College of Agriculture, Central Agricultural University, Imphal, Manipur, India

ARTICLE INFO

Keywords:
Tricholoma matsutake fungi biomass
Chitosan
Functionalization
Adsorption
Methylene blue

ABSTRACT

The study evaluates the adsorption efficiency of Tricholoma matsutake fungi biomass (TMF) and its chitosan-functionalized form (TMFC) for the removal of methylene blue (MB) from aqueous solutions. The physico-chemical, morphological properties of the synthesized adsorbent was characterized using various techniques, including FTIR, SEM, BET respectively. The surface functionalization of TMF with chitosan substantially increased the surface area of 18 folds from 2.157 m^2/g (TMF) to 37.03 m^2/g (TMFC). Adsorption experiments were performed to evaluate the dye removal efficiency under various conditions such as pH (2–12), adsorbent dosage (0.01 g–0.05 g), contact time (0–300 min), agitation speed (100–500 rpm). The equilibrium adsorption data were fitted with different adsorption isotherm models namely Langmuir, Freundlich; and the kinetics adsorption data were fitted with pseudo-first order, pseudo-second order models. The chitosan modification significantly enhanced the adsorption capacity of TMF, with TMFC demonstrating an adsorption capacity of 160.25 ± 6.207 mg/g at pH 8.0, compared to 59.42 ± 2.058 mg/g at pH 6.0 for the unmodified TMF. Finally, the sorbent material TMF, TMFC is regenerated by an acidic eluent (HCl) with a maximum desorption percentage of ca.90 % (TMFC) and ca.60 % (TMF). Lastly, and the synthesize sorbent material TMFC can be reused for five successive cycles, while TMF is utilized to a maximum of 2 cycles. The findings of this study highlight the potential of TMFC as an effective and sustainable adsorbent for the removal of MB from aqueous solutions.

1. Introduction

The rapid industrialization and urbanization over the past century have significantly intensified environmental pollution, particularly affecting water resources. Synthetic dyes, including methylene blue (MB), are among the most problematic pollutants due to their persistence and resistance to biodegradation. As a synthetic cationic dye, MB is extensively used in various industries, including textiles, leather, and paper manufacturing. In the textile industry, MB is commonly used for dyeing cotton, wool, and silk, owing to its strong affinity for natural fibers and its vibrant blue hue. The pharmaceutical sector also employs MB for its medicinal properties, including its use as a treatment for methemoglobinemia and as a diagnostic agent in various medical procedures. Upon discharging this MB into water bodies without proper treatment, it causes severe ecological harm. MB absorbs light, reducing water transparency and limiting photosynthetic activity in aquatic environments, which disrupts the oxygen balance and affects aquatic organisms. From a human health perspective, exposure to methylene blue can cause irritation of the skin, eyes, and respiratory tract, with potential long-term risks including carcinogenicity, mutagenicity, and genetic damage. The presence of such dyes not only deteriorates the visual quality of water but also poses serious risks to aquatic ecosystems and human health at elevated concentrations [1]. Conventional dye removal methods such as coagulation, flocculation, adsorption, sedimentation, and membrane filtration frequently generate secondary sludge and demand significant energy input [2]. Among which adsorption has gained

---

* Corresponding authors.
E-mail addresses: garkiran@yuntech.edu.tw (A.R.K. Gollakota), shucm@yuntech.edu.tw (C.-M. Shu).

https://doi.org/10.1016/j.molliq.2025.127305
Received 29 October 2024; Received in revised form 7 February 2025; Accepted 5 March 2025

prominence as a highly efficient and straight forward alternative, with notable potential for regeneration. This technique facilitates the transfer of dye molecules (adsorbates) from the aqueous phase to the surface of a solid adsorbent through physical or chemical interactions. The effectiveness of this process is contingent upon the selection of an adsorbent characterized by high capacity, selectivity for the target dye, rapid adsorption kinetics, and the capability for regeneration across multiple cycles [3–9].

In recent years, there has been a growing focus on developing sustainable and eco-friendly adsorbents, with natural and bio-based materials gaining prominence due to their abundance, low cost, renewability, and minimal toxicity. Fungi are promising adsorbents for dye removal due to their polysaccharide-rich cell walls, which contain functional groups that facilitate strong interactions with dye molecules. Their abundance, rapid growth, high surface area, biodegradability, and low cost make fungi an effective and sustainable option for wastewater treatment. Tricholoma matsutake (TMF) is one such material offers several advantages as an adsorbent, including its sustainability as a naturally occurring, renewable resource with minimal environmental impact. It is biodegradable, making it an eco-friendly option, and its porous structure with functional groups like hydroxyl, amino, and carboxyl enhances adsorption, particularly for cationic dyes such as methylene blue. The material is cost-effective and can be used in large quantities, offering significant yield when properly cultivated or harvested. However, challenges include variability in adsorption capacity, potential for microbial contamination, which could increase operational complexity. Additionally, the adsorption kinetics may be slower compared to synthetic adsorbents, requiring longer contact times for effective dye removal.

Chitosan, derived from the deacetylation of chitin, is a cationic biopolymer recognized for its biocompatibility, biodegradability, and non-toxicity [10]. The amino (NH_2) and hydroxyl (OH) groups in chitosan facilitate strong interactions with dyes through electrostatic attractions, hydrogen bonding, and complexation, thus improving adsorption capacity [11]. When combined with chitosan, which introduces additional carboxyl and hydroxyl groups, the functionalized fungi exhibit enhanced dye removal efficiency due to increased electrostatic binding and chelation capabilities [12]. This research introduces a novel, eco-friendly approach for methylene blue (MB) removal by developing chitosan-functionalized Tricholoma matsutake fungal biomass as an effective adsorbent. The innovation lies in the dual functionalization of naturally abundant fungal biomass with chitosan, enhancing its adsorption capacity, reusability, and stability compared to traditional adsorbents. Through advanced characterization and optimization of functionalization strategies, this study provides scalable, sustainable solutions for efficient dye removal. The integration of comprehensive adsorption studies using established models Langmuir, Freundlich, and pseudo-first/second-order kinetics offers valuable mechanistic insights into the adsorption process and provides a predictive framework for real-world wastewater treatment applications. The inclusion of desorption-regeneration cycles further underscores the sustainability of this approach, establishing a transformative pathway for dye remediation. Ultimately, this research pioneers a sustainable, high-performance solution for wastewater treatment, setting the stage for future innovations in complex wastewater environments.

2. Materials and methods

The reagents and chemicals namely NaOH, 90 % deacytelated chitosan (200–400 MPa.s) methylene blue (MB) dye (≥82 % dye composition), acetic acid (≥99 % purity), HNO_3, ethylenediaminetetraacetic acid (EDTA) used in the current experimentation were of analytical grade and obtained from Sigma-Aldrich Taiwan.

2.1. Biomass feedstock preparation

TMF feedstock were collected from the YunTech (National Yunlin University of Science and Technology) campus. To ensure cleanliness, they were meticulously washed in running water to remove any adhering debris. Following this initial cleaning step, a two-stage drying process was performed in a furnace 50 °C for 24 h to ensure complete removal of any remaining moisture traces. Finally, the fully dried TMF was crushed into a fine powder for further experimentation. Since the pH of the raw TMF is in the range of 4.5–5.5, it was repeatedly washed with the DI until the obtainment of neutral pH. The material is further dried and ready for further use.

2.2. Preparation of the dye solution

MB dye was dissolved in 1000 mL of double distilled water to prepare a stock solution with a concentration of 1000 mg/L. Sequentially diluting the stock solution with double distilled water yielded dye solutions with concentration ranges between 100 and 1000 mg/L for use in further experimentation.

2.3. Synthesis of CHI/TMF (TMFC) bio composite

The acquisition of high-quality chitosan powder, characterized by specific molecular weight and degree of deacetylation, is paramount for ensuring the success of subsequent experimental procedures. Dissolve 3 g of chitosan in 2 % (v/v) acetic acid, and continuously stirred the solution until the chitosan is completely dissolved and a clear solution is obtained and designated as pure chitosan solution (PCS) and required for further use in the following steps. The PCS solution prepared in the previous step was combined with air-dried TMF in a 1:1 ratio. The mixture was then stirred on a magnetic stirrer for 24 h at room temperature to ensure the thorough functionalization of the TMF into the PCS solution. To ensure the PCS was completely dissolved and that TMF was effectively incorporated into the CHI matrix, this extended duration was implemented. The choice of the 1: 1 was considered after several trial and error ratios and found that 1:1 seems to the optimal ratio yielding better results. Upon achieving complete dissolution of the TMF within the chitosan gel matrix (PCS), the resulting mixture was dispensed into 100 mL solution of 2 M NaOH [13] equilibrated at 30 °C [14], and the resultant mixture was washed thoroughly with DI water to remove the contaminants and external traces of NaOH and stored in fresh DI water (100 mL) left for the further steps.

3. Batch adsorption assays

A series of batch adsorption experiments were conducted to evaluate the removal efficiency of MB dye. A stock solution of the dye was prepared at a concentration of 1000 mg/L. Subsequent dye solutions with varying concentrations were obtained by diluting the stock solution. For each experiment, 0.03 g (TMF), 0.02 g (TMFC) of the adsorbent was added to 10 mL of the prepared dye solution in polypropylene tubes. The mixtures were incubated at natural pH (unadjusted) and 25 °C for 90 min (TMF), and 60 min (TMFC) to allow for adsorption. Following incubation, the supernatant fractions containing the unabsorbed dye were separated from the adsorbent by decantation. The concentration of MB dye remaining in the supernatant was then quantified using a UV–vis spectrophotometer at a wavelength of $\lambda = 664$ nm. The adsorption capacity (q_e, mg/g) of the adsorbent and the desorption efficiency were calculated using Eqs. (1) and (2), respectively.

$$Q_e = \left[\frac{C_i - C_f}{m}\right] \times V \tag{1}$$

$$\text{Desorption}(\%) = \frac{desorption}{adsortpion} \times 100 \tag{2}$$

where C_i, C_f, m, and V denote the initial dye concentration, equilibrium dye concentration, the mass of the adsorbent used and the volume of the experimental solution, respectively. All the experimental studies were performed thrice to check the reliability of the experimental values, and the average values were presented herein.

4. Sample characterization

A comprehensive suite of characterization techniques were performed to elucidate the physicochemical properties of the sorbent materials, namely TMF and chitosan-functionalized TMF (TMFC). The textural properties were assessed through N_2 adsorption–desorption isotherms using a surface area pore analyzer (Micrometrics ASAP 2060). Prior to analysis, samples were meticulously degassed at 150 °C for 20 h to eliminate any adsorbed contaminants that could influence measurement outcomes. The micropore and mesopore areas and volumes were calculated by integrating the pore size distribution curve, while the Brunauer–Emmett–Teller (BET) specific surface area (SBET) was determined using the established BET equation, providing a quantitative measure of the total surface area accessible for gas adsorption. Surface morphology of both TMF and TMFC was analyzed using an ultra-high-resolution thermal field emission scanning electron microscope (JEOL, JSM-7610F Plus). Prior to scanning electron microscopy (SEM) analysis, specimens were coated with a thin layer of gold via a sputter coater to ensure conductivity. Functional group identification was conducted using Fourier transform infrared spectroscopy (FTIR, Perkin-Elmer Spectrum One), equipped with a DTGBr detector and employing KBr as a beam splitter, with a scanning range of 400–4000 cm^{-1}. Adsorption studies were performed using a UV–VIS spectrophotometer (Perkin-Elmer Lambda 850), utilizing a quartz cell with a 1.0 nm path length at a wavelength of 664 nm. This multifaceted characterization approach, integrating diverse analytical techniques, provided extensive insights into the physicochemical properties of both pristine and modified sorbent samples, establishing a solid foundation for their potential applications across various fields.

5. Results and discussion

5.1. Characterization techniques

5.1.1. BET analysis

The surface area and pore structure of TMF and TMFC were systematically analyzed using Brunauer-Emmett-Teller (BET) and Barrett-Joyner-Halenda (BJH) methods to evaluate their potential as adsorbents for MB dye molecules. For the TMF, BET analysis revealed a specific surface area of 2.157 m^2/g (see Table 1).

The nitrogen adsorption–desorption isotherm displayed a Type IV (see Fig. 1) profile according to the IUPAC classification, indicating a mesoporous material. The distinct Type H3 hysteresis loop observed is characteristic of material with slit-shaped pores and partial mesopore filling [15]. Further, the BJH pore size distribution analysis confirmed that the majority of pores fell within the mesopore range of 2–50 nm, thereby validating the mesoporous nature of the biomass. The calculated pore volume was 0.0135 cm^3/g, reflecting its capacity for adsorbate accommodation [16]. Following chitosan functionalization, BET analysis revealed a significant increase in specific surface area to 37.03 m^2/g (see Table 1), highlighting an enhancement in the biomass adsorption capacity. While the adsorption isotherm retained its Type IV classification, the observed modifications in hysteresis loop indicated alterations in pore structures resulting from chitosan incorporation. The BJH analysis of the chitosan-functionalized biomass demonstrated an increase in pore volume to 0.1468 cm^3/g compared to the unmodified biomass. This broadening of the pore size distribution suggests that chitosan functionalization expanded the mesopore structure and introduced additional adsorption sites [17]. The broadening of the pore size distribution upon chitosan functionalization is attributed to significant structural and chemical alterations on the fungal biomass surface. Chitosan, a polysaccharide comprising β-(1 → 4)-linked D-glucosamine and N-acetyl-D-glucosamine units, is enriched with functional amino ($-NH_2$) and hydroxyl (–OH) groups, which exhibit high reactivity during the functionalization process. These functional groups engage in hydrogen bonding, electrostatic interactions, and possibly covalent grafting with reactive sites on the fungal biomass, including carboxyl and hydroxyl groups. Such interactions may disrupt the original microporous structure, leading to the expansion of mesopores as chitosan chains integrate into and partially bridge smaller pores. Further, the grafting process introduces additional adsorption sites due to the amino groups' nucleophilic nature and electron-donating capacity, enabling coordination interactions with methylene blue, a cationic dye. This chemical modification enhances the surface's electrostatic affinity and improves accessibility to adsorption sites, particularly for larger dye molecules. Furthermore, the functionalization increases pore connectivity and may induce swelling of the polymeric network, contributing to a broader pore size distribution.

Table 1
Morphological features of TMF, and TMFC.

Adsorbent	SBET surface area (m^2/g)	Total pore volume (cm^3/g)
Raw fungal biomass (TMF)	2.157	0.0135
Chitosan-functionalized fungal biomass (TMFC)	37.03	0.1468

The modified hysteresis loop further implies improved pore connectivity and accessibility, which are critical for enhanced adsorption performance [18]. These BET and BJH findings demonstrate that chitosan functionalization significantly alters the surface and pore characteristics of TMF biomass. The observed increase in specific surface area and the expanded pore size distribution indicate that chitosan not only increases the pore volume but also creates new adsorption sites, thereby improving the biomass efficacy in adsorbing MB dye.

5.1.2. FTIR analysis

Fourier-transform infrared (FTIR) spectroscopy provides a comprehensive analysis of the chemical composition and functional groups in both TMF and its counter TMFC. The FTIR spectrum of chitosan (Fig. 2a) displays prominent peaks, notably a broad O–H and N–H stretching band around 3435–3462 cm^{-1}, characteristic of its polysaccharide structure. A peak at 1798 cm^{-1} suggests the presence of N-acetyl groups (amide I), while those at 2918 and 2512 cm^{-1} are assigned to C–H stretching vibrations. Additionally, peaks at 1420, and 873 cm^{-1} reflect C–O stretching and other skeletal vibrations, providing a comprehensive profile of chitosan vibrational modes. Further, Fig. 2b reveals several critical peaks of unmodified TMF that elucidate its structural characteristics. The peak at 862 cm^{-1} is attributed to out-of-plane bending vibrations of C–H bonds in aromatic rings, indicative of phenolic or aromatic compounds inherent in the fungal cell walls [19], which are essential for the biomass's structural integrity and functional properties.

The peak at 1021 cm^{-1} corresponds to C–O stretching vibrations associated with alcohols, ethers, and polysaccharides, signifying the presence of carbohydrate structures such as cellulose or chitin crucial for the structural matrix of the fungal cell walls [20]. The peak at 1156 cm^{-1} represents C–O stretching within glycosidic linkages, characteristic of chitosan or cellulose, highlighting the complex carbohydrate network within the biomass [21]. The 1384 cm^{-1} peak is attributed to C–H bending vibrations of methyl groups (CH_3), a characteristic feature found in various components of the materials, such as fatty acids, lipids and other aliphatic structures. While the presence of this peak may suggest the presence of lipids or fatty acids, it is not exclusive to them, as it can also arise from methyl groups in other components of the biomass, including chitosan and carbohydrates [22]. The peak between 1600–1700 cm^{-1} signifies the C=O stretching vibration of the Amide I

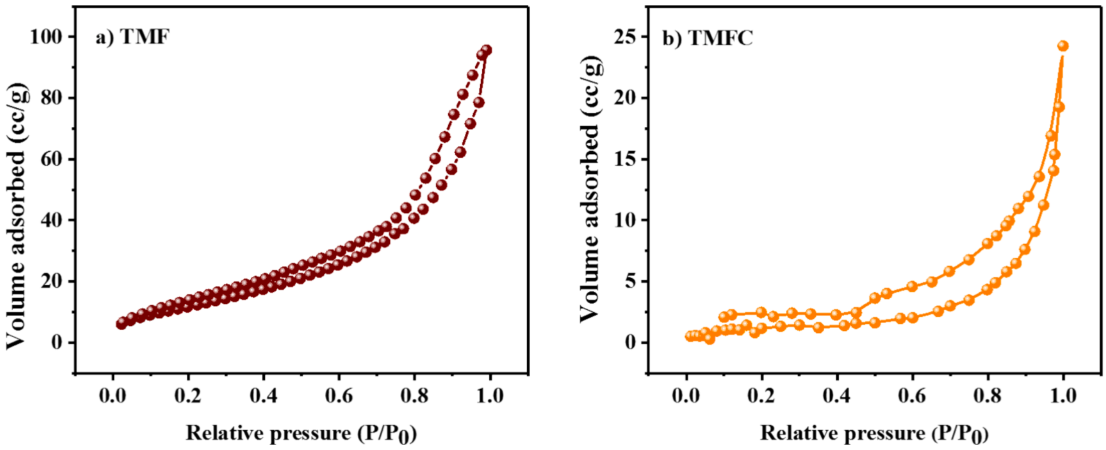

Fig. 1. Spectra of N_2 adsorption–desorption isotherm (a) fungal biomass TMF, (b) chitosan functionalized fungal biomass TMFC.

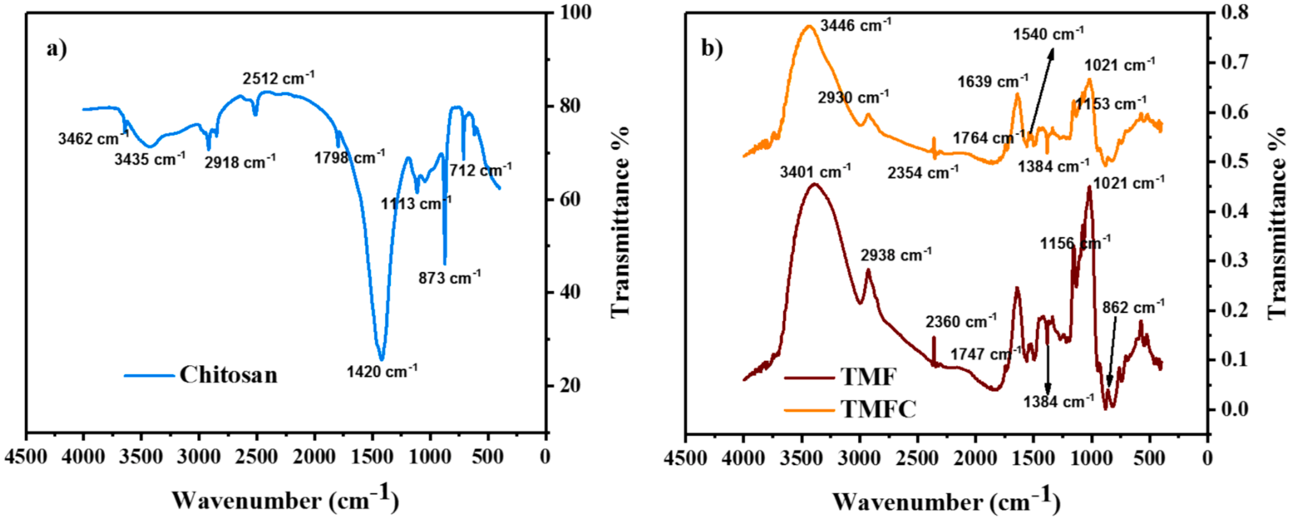

Fig. 2. FT-IR spectra of (a) chitosan, (b) TMF, TMFC.

band, indicative of proteins or peptides, which are vital for various biochemical functions [23]. The 1747 cm^{-1} peak corresponds to –C=O (ester) stretching vibrations from aldehydes and ketones, reflecting carbonyl groups involved in biochemical and chemical reactivity [24]. The peak at 2360 cm^{-1} is most likely due to the presence of atmospheric CO_2 [25] while the 2938 cm^{-1} peak is an indicative of C–H bonds in aliphatic chains, typically from lipids or fatty acids, indicating the presence of hydrophobic components in the biomass. This peak is commonly observed in chitosan-functionalized biomass, where the modification introduces lipid-like groups, contributing to the materials increased hydrophobicity [26].

In contrast, the FTIR spectrum of TMFC (Fig. 2b) highlights significant modifications due to chitosan integration. The peak at 1021 cm^{-1} retains its association with C–O stretching vibrations, indicating that carbohydrate structures like cellulose or chitosan remain in the biomass [27]. The peak at 1153 cm^{-1} confirms the persistence of C–O–C stretching within glycosidic linkages, characteristic of chitosan or cellulose, affirming the continuity of these polysaccharides after chitosan functionalization [28]. The peak at 1384 cm^{-1} continues to represent C–H bending vibrations linked to methyl groups, indicating the presence of fatty acids or lipids [29]. Notably, the new peak at 1325 cm^{-1} signifies C–N stretching vibrations, confirming the successful incorporation of chitosan into the biomass matrix [30], and 1639 cm^{-1} peak indicates the C=O from chitosan on these structures [31]. The peak at 1746 cm^{-1} reflects C=O stretching vibrations associated with carbonyl groups [32], peaks at 2354 cm^{-1} and 2930 cm^{-1} represent C–H stretching vibrations, indicating non-polar components and fatty acids [33,34]. Lastly, the peaks at 3401 cm^{-1}, 3446 cm^{-1} can be attributed to both O–H and N–H stretching vibrations. While O–H stretching typically indicates hydrogen bonding and may be linked to increased surface hydrophilicity, the N–H stretching from the amine groups in chitosan can also contribute to these peaks. Additionally, the bending vibration of N–H is typically observed around 1540 cm^{-1}, further supporting the involvement of amine groups in the functionalization process [35].

In summary, the FTIR analysis reveals distinct structural and functional group variations between TMF and TMFC. A notable shift from 3446 cm^{-1} to 3401 cm^{-1} in TMFC suggests the introduction of a hydroxyl group (O–H), which is either absent or less pronounced in TMF. Minor shifts in the C–H stretching vibration (from 2930 cm^{-1} to 2938 cm^{-1}) and C=O stretching (from 1746 cm^{-1} to 1747 cm^{-1}) in TMFC indicate subtle changes in the chemical environment of these groups. The appearance of a C=C bond stretching vibration around 1639 cm^{-1}, shifting into the 1600–1700 cm^{-1} range in TMFC, further highlights the transformation of functional groups compared to TMF. While some peaks remain relatively unchanged (e.g., 1384 cm^{-1} and 1021 cm^{-1}), the emergence of a new band at 862 cm^{-1} in TMFC suggests the presence of an additional functional group, which is either absent or less prominent in TMF. Collectively, these spectral shifts provide compelling evidence of significant structural and chemical modifications in TMFC, reflecting its altered functional properties, demonstrating enhanced potential for applications in environmental remediation.

5.1.3. SEM analysis

Scanning electron microscopy (SEM) was utilized to examine the surface morphology and structural modifications of TMFC and its subsequent functionalization with chitosan polymer (TMFC). The SEM images (see Fig. 3a) of unmodified TMF reveal a distinctly regular and porous surface, characterized by an intricate network of fungal hyphae with a fibrous and textured appearance.

This natural morphology, marked by the interlacing of fungal and mycelial networks, provides a significant surface area, which is crucial for its ecological roles, including nutrient absorption and interaction with the environment.

Following chitosan functionalization, substantial morphological changes were observed. Fig. 3b (TMFC) presents a rougher surface with pronounced cracks, crevices, and folds, indicating a significant increase in surface irregularity compared to Fig. 3a. Further, Fig. 3C (TMFC) displays a surface that, while still rough, appears less dense and more porous, with larger voids or cavities than those Fig. 3a suitable for the better adsorption tendency. (see Fig. 3(b and c)). In summary, SEM analysis provides a comprehensive view of the structural changes induced by chitosan functionalization. The transformation from the rough, fibrous surface of TMF to an enhanced adsorption sites surface of TMFC underscores the effectiveness of chitosan in modifying the biomass surface characteristics. This transition highlights the potential of TMFC for various applications, including environmental cleanup and as a component in bio-composite materials. Lastly, Fig. 3d highlights the SEM micrograph of the TFMC after the desorption studies. The Image reveals that the surface active sites are intact after the first adsorption cycle with roughness and with very mild surface changes. Thus, the adsorbent can be reused for the successive cycles and the details are provided in the subsequent sections. The detailed SEM observations are pivotal for understanding the functional enhancements brought about by chitosan modification and underscore its potential for optimized use in practical applications.

5.2. Adsorption experiments

5.2.1. Influence of pH

To interpret the influence of solution pH on MB dye adsorption onto sorbent materials TMF and TMFC, a series of adsorption experiments were performed with MB dye concentration of 300 mg/L across a pH range of 2 to 12. The pH levels of the solutions were carefully adjusted with 0.1 N HCl and 0.1 N NaOH to ensure accuracy. For each pH condition, 0.03 g of TMF and 0.02 g TMFC was introduced into the solutions, followed by agitation for 90 min for TMF and 60 min for TMFC to reach equilibrium. The adsorption capacities were evaluated by analyzing the residual MB concentrations in the supernatant. As depicted in Fig. 4a, the adsorption of MB increased significantly with increasing pH in both the sorbent materials TMF (15.98 mg/g, pH = 6) and TMFC (61.21 mg/g, pH = 8). This increasing trend of adsorption with pH is attributed to improved electrostatic interactions between the cationic MB dye and the adsorbent surfaces [36]. Additionally, increasing pH promotes the deprotonation of acidic functional groups on

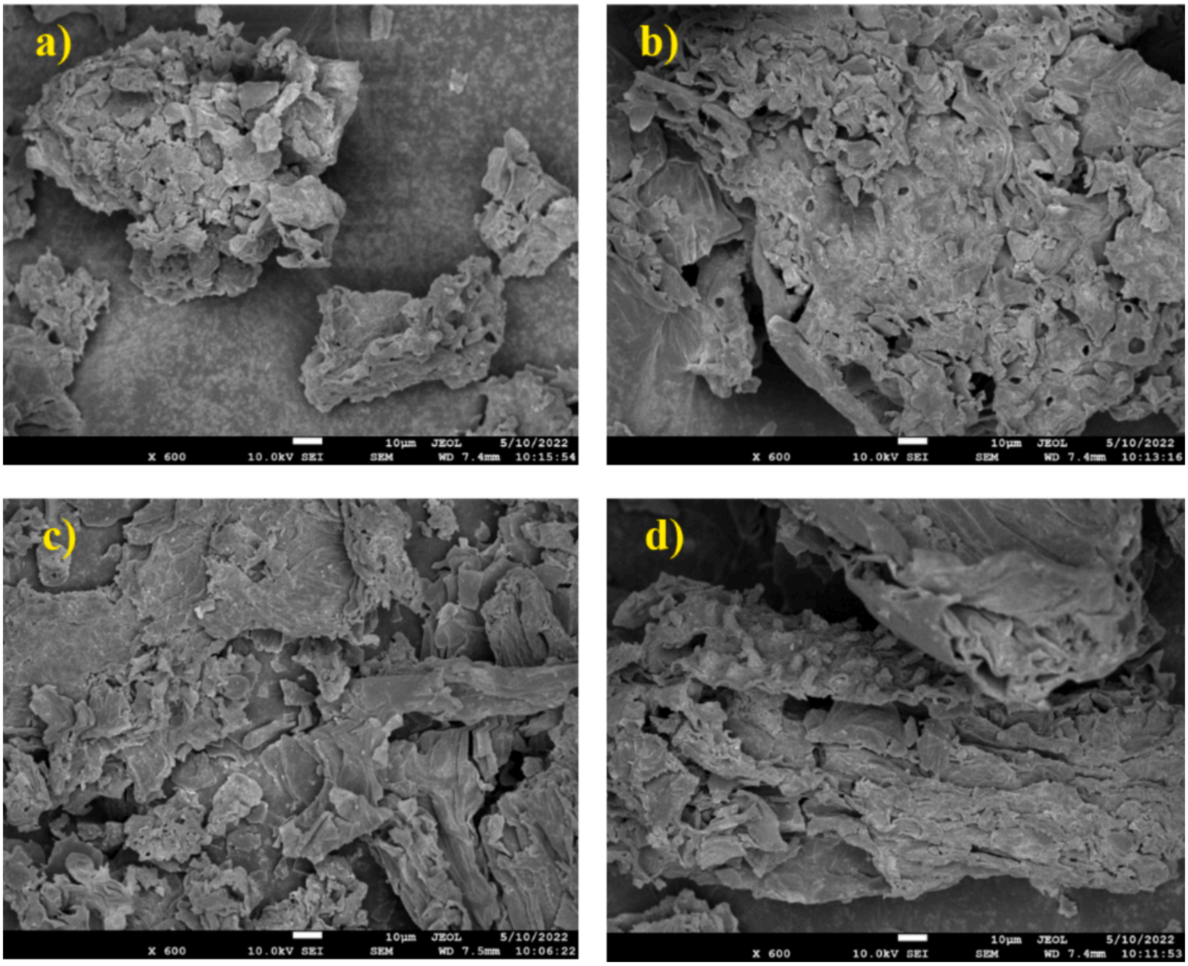

Fig. 3. SEM micrographs of (a) TMF, (b and c) TMFC, d) after desorption.

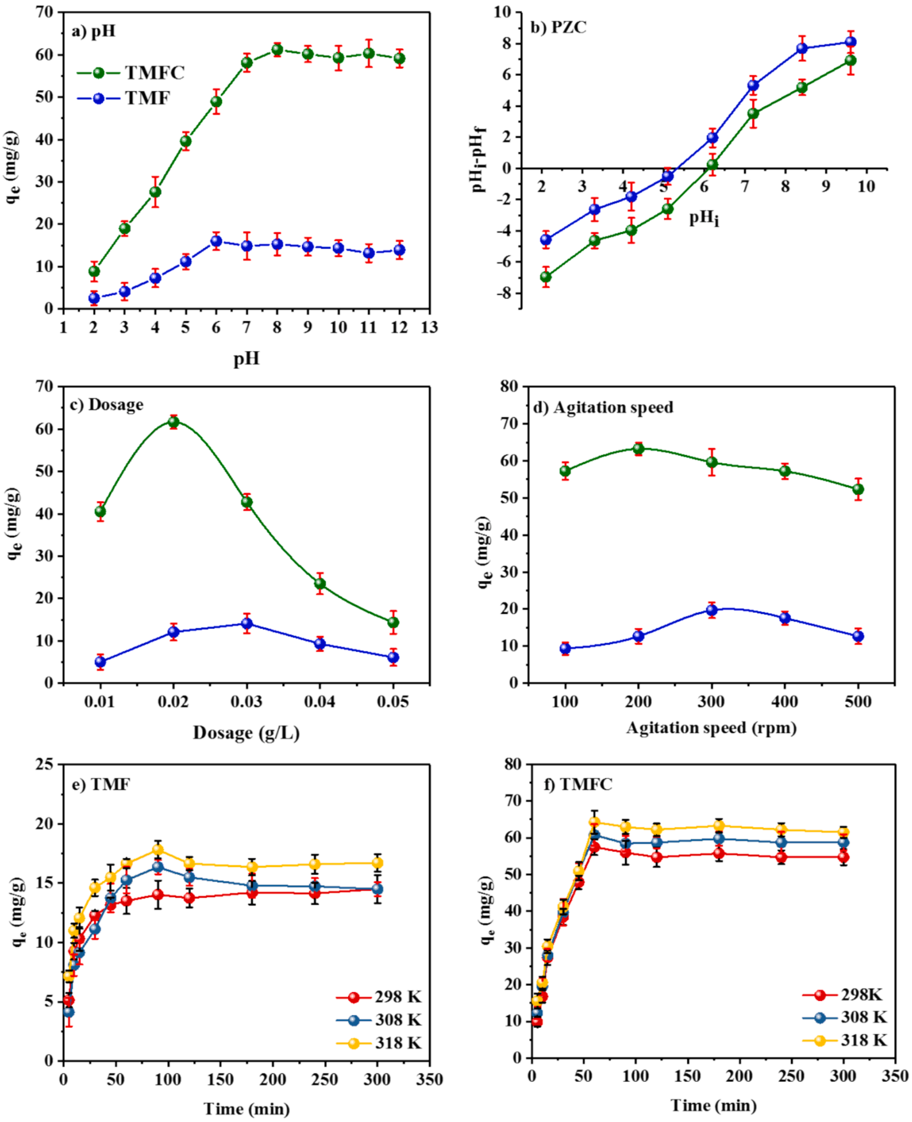

Fig. 4. Effect of process parameters on adsorption capacity (a) pH, (b) pzc, (c) dosage, (d) agitation speed, (e) effect of time using TMF, (f) effect of time using TMFC.

the adsorbents (TMF, TFMC), thereby increasing the negatively charged sites that attract the positively charged MB dye more effectively [37]. However, in the case of TMF optimal MB adsorption occurred at pH = 6, due to the sorbents increased positive surface charge in acidic conditions, which enhances electrostatic attraction with the cationic dye. Whereas, TFMC showcased the highest adsorption at pH = 8, indicating the inclusion of amino groups upon functionalizing with chitosan that extends the pH range over which the biomass maintains a negative surface charge, thereby maximizing electrostatic interactions with the MB dye [38]. Further increasing the pH values beyond 6 (TMF) and 8 (TMFC), there observed a plateau indicating the unavailability of the active sites for adsorption and hence the declining trend is seen. From

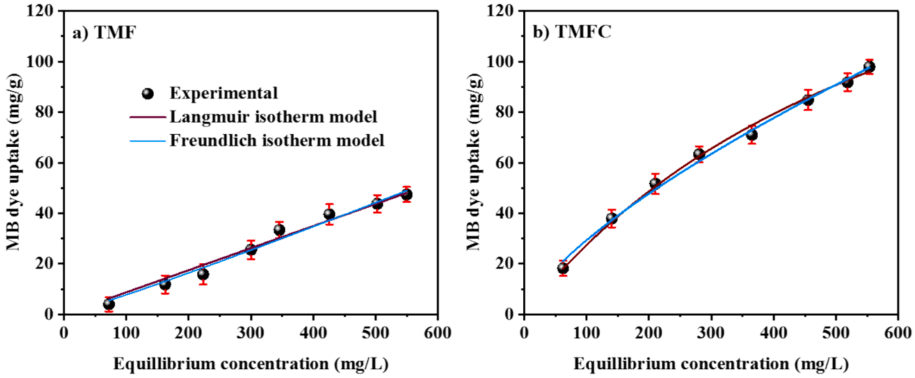

Fig. 5. Non-linear adsorption isotherm studies varied with dye concentration (a) TFM, (b) TFMC.

the pH studies it is clearly evident that functionalizing TFM with chitosan offers superior MB dye molecule removal efficiency compared to raw TMF.

5.2.2. Influence of PZC

The knowledge on point of zero charge (PZC) is vital predicting the adsorbate-adsorbent interactions as well as aiding to optimize the adsorption conditions. From Fig. 5, it is seen that PZC of TMF was noted to be 5.5, i.e., less than the pH of optimal adsorption (pH = 6), indicating the net surface charge is negative, that leads to the electrostatic interaction of cationic dyes (see Fig. 4b). This negative charge is mainly due to the deprotonation of the major functional groups, such as amine groups (–NH_2), and hydroxyl groups (–OH) present in TMF and validated through FTIR peaks. However, chitosan containing amino groups with pKa values approximately 6.5 play a crucial role in its interaction with cationic dyes like methylene blue (MB). At neutral to slightly alkaline pH levels, the amino groups can become protonated (–NH_3^+), imparting positive charges to the biomass surface [38]. This positive charge could limit interactions with other cationic species. However, if other negatively charged groups are present on the biomass (e.g., carboxyl groups observed from FTIR range 1600–1700 cm^{-1}), they could promote electrostatic attraction with the cationic MB dye, enhancing its adsorption. FTIR analysis of the TMFC reveals new peaks associated with –NH_2 stretching, indicating successful functionalization and an increase in available amino groups [39]. This modification allows the TMFC to effectively capture MB at neutral to alkaline pH levels, contrasting with TMF, which is predominantly effective under acidic conditions due to its natural positive charge below its point of zero charge (PZC) (see Fig. 4b). By shifting the PZC upward and increasing the surface positive charge, chitosan modification broadens the effective pH range for MB adsorption, enabling the biomass to function as a more versatile and effective adsorbent. This adaptability is essential for environmental applications focused on the removal of cationic dyes from wastewater.

5.2.3. Effect of adsorbent dosage

The study examined the impact of adsorbent dosage on the adsorption of methylene blue (MB) dye onto TMF and TMFC adsorbents. The experiment were performed using 0.01–0.05 g/L of the TMF and 0.01–0.05 g/L of the TMFC as adsorbent dosages each to treat 30 mL of a MB dye solution with an initial concentration of 300 mg/L [40]. The results revealed an optimal uptake of MB dye by the TMFC compared to TMF, followed by a gradual declining pattern with both sorbents (see Fig. 4c). The initial increase in the uptake is due to the availability of active sites and higher sorbate-sorbent interactions, while the decrease refers to the saturation of the sites and hence lowering the interactions [41]. Upon analysis, it was noted that TMFC performed better adsorption of MB dye molecules at 0.02 g/L, and TMF was optimal at 0.03 g/L.

5.2.4. Effect of agitation speed

The effect of agitation speed on the sorption capacity and efficiency of MB dye adsorption onto TMF and TMFC sorbent materials was systematically studied at different agitation speeds ranging between 100 and 500 rpm. The results indicated a marginal effect on sorption capacity, which ranged between 10 and 20 mg/g in case of TMF where as it is between 40 and 67 mg/g for TMFC respectively. (Fig. 4d). Agitation speed impacts the equilibrium time, with lower speeds necessitating longer contact times. In the present context, a constant contact time of 300 min was employed. It was noticed that an agitation speed of 200 rpm seems favorable for the maximum adsorption of MB on TMF whereas, it was 300 rpm in case of TMFC respectively. The primary role of agitation speed in this context is to control uptake kinetics by influencing the resistance to film diffusion [42]. The increasing adsorption with the agitation speed is ascribed due to the distribution of dye molecules within the bulk solution and the formation of the external boundary film around adsorbent particles. In batch experiments, changing the agitation speed helps check if external resistance is important. If dye molecule mass transfer controls the adsorption rate, the agitation speed will significantly affect the uptake rate [43].

5.2.5. Effect of contact time

Fig. 4e explores the critical influence of contact time on the adsorption efficiency of MB dye molecule using TMF and TMFC. In this experiment, 0.03 g of TMF and 0.02 g of TMFC was used to treat 30 mL of an MB dye solution with an initial concentration of 300 mg/L. The results reveal an intriguing trend: a significantly higher adsorption capacity at the initial stages (0–60 min for TMF; 0–100 min for TMFC), followed by a plateau in the adsorption rate. This behavior can be attributed to the availability of active sites on the TMFC surface i.e., during the initial phase, the sorbent molecules have abundant active sites readily accessible to MB molecules, facilitating rapid adsorption. As the process continues, these active sites become increasingly occupied by MB molecules, similar to a filling-up process. This saturation effect reduces the number of available sites, leading to a slower adsorption rate for the remaining MB molecules [44]. Fig. 4 (e and f) visually confirms this relationship, showing a notable increase in MB removal of 14.03 mg/g – 17.82 mg/g (TMF at variable temperatures) within the first 90 min, indicating a period of rapid adsorption. After this rapid phase, the adsorption rate plateaus, with the removal efficiency reaching a maximum of 17.8 mg/g. Similarly for TMFC the adsorption capacity raised from 57.42–64.25 mg/g in the first 60 min, and attaining equilibrium thereafter. This plateau suggests the saturation of available active sites on the TMFC surface, indicating that extending the contact time beyond this point does not significantly enhance removal efficiency. Therefore, Figure Fig. 4 (e and f) underscores the importance of optimizing contact time for effective MB removal using TMFC over TMF. This understanding can guide the development of efficient MB removal processes, ensuring optimized resource utilization.

6. Isotherms, kinetics and thermodynamic studies

6.1. Adsorption isotherms

To elucidate the interaction between the adsorbate (MB dye) and the adsorbents (TMF, TMFC) adsorption isotherm models were employed. These models provide valuable insights into the bio sorption mechanism by describing the equilibrium relationship between the amount of adsorbate adsorbed and its concentration in the surrounding solution. The experimental data obtained from the batch adsorption experiments were analyzed using the established isotherm models of Langmuir, Freundlich.

The Langmuir isotherm provides a theoretical framework for ideal monolayer adsorption based on several key assumptions. It posits that adsorption occurs in a single layer on uniform active sites of the adsorbent, with each site having identical energetic attraction for the adsorbate molecules, thus minimizing interactions between them. The model assumes independent adsorption, meaning that adsorbed molecules do not interact laterally, and depicts adsorbate immobility, where once adsorbed, molecules cannot migrate across the surface. These assumptions create a simplified model for analyzing adsorption behavior [45]. The Langmuir model predicts that adsorption increases linearly with initial adsorbate concentration until it reaches a saturation point, forming a complete monolayer on the surface, after which the adsorbed amount remains constant. Although the specific equation is not included here, it mathematically describes the relationship between the adsorbed quantity and initial adsorbate concentration, with a non-linear form of the Langmuir isotherm model given by

$$q_e = \frac{q_m K_L C_e}{1 + K_L C_e} \tag{3}$$

In contrast to the Langmuir model, the Freundlich isotherm provides a framework for understanding adsorption on heterogeneous surfaces, recognizing that adsorption sites have varying binding strengths. Initially, sites with stronger attraction are occupied, followed by those with weaker binding as the surface fills. The Freundlich isotherm is mathematically expressed as an exponential equation, indicating that as the concentration of adsorbate in the bulk solution increases, the amount adsorbed on the surface also rises exponentially. This reflects the surface's energetic heterogeneity and the gradual occupation of sites with decreasing binding strength. The non-linear form of the Freundlich isotherm model can be mathematically represented as follows.

Mathematically, the Freundlich isotherm is expressed as an exponential equation which reflects the notion that as the concentration of the adsorbate in the bulk solution increases, the amount of adsorbate adsorbed onto the surface also increases exponentially [46]. This exponential dependence accounts for the energetic heterogeneity of the surface and the progressive filling of sites with decreasing binding strength.

The mathematical expression of non-linear form of Freundlich isotherm model is as follows

$$q_e = K_f C_e^{1/n} \tag{4}$$

In the present study, Langmuir and Freundlich adsorption isotherms were used to determine the adsorption capacity of the equilibrium data for MB dye molecule on sorbents TMF and TMFC. It is observed that as the concentration increases, the driving force along the concentration gradient also increases, which in turn enhances the diffusion of MB molecules in the solution and facilitates the adsorption onto the surface of the TMF and TMFC. Fig. 5 (a-b) present the Langmuir and Freundlich non-linear regression adsorption isotherm fitting curves of TMF, TMF adsorbing MB dye molecules respectively. The corresponding parameters for both isotherms are summarized in Table 2. From the table it was noted that the maximum monolayer adsorption capacity (q_m) was determined to be 59.42 ± 2.058 mg/g for TMF and it is 160.25 ± 6.207 mg/g for TMFC.

On the other hand, the Freundlich model provided a constant *N* value of less than 1, indicating favorable adsorption conditions. These findings highlight the reliability and applicability of the Langmuir and Freundlich models in describing the adsorption behavior of MB dye onto TMFC than TMF. Further, the Langmuir model, with its high q_m value, suggests a significant adsorption capacity, while the Freundlich model indicates a strong affinity between the dye molecules and the adsorbent, corroborating the effectiveness of the adsorption process. In addition, the high values of the estimated coefficient of determination (R^2) confirmed the acceptability and suitability of the Langmuir and Freundlich isotherm models for describing the adsorption process. It was observed from the analysis, the adsorption capacity of TMF up taking MB dye molecule is 59.42 ± 2.058 mg/g, while the TMFC reported 160.25 ± 6.207 mg/g. The reason ascribed for the higher adsorption of TMFC is due to inducement of functional groups and the morphological properties such as pore volume, pore diameter, surface area etc. upon functionalizing with chitosan polymer. In addition, a detailed summary of the literature pertaining MB dye adsorption by various adsorbents are presented in Table 3.

Table 2
Equilibrium modeling of data for the removal of MB dye using TMF, TMFC.

Langmuir isotherm	Value	Freundlich isotherm	Value
TMF			
q_m (mg/g)	59.42 ± 2.0586	K_f (mg/g)	0.188 ± 0.0249
K_L (L/mg)	0.0005 ± 0.00007	N	1.240 ± 0.1624
R^2	0.9964	R^2	0.9623
TMFC			
q_m (mg/g)	160.25 ± 6.2071	K_f (mg/g)	1.775 ± 0.5324
K_L (L/mg)	0.0016 ± 0.0016	N	1.710 ± 0.2481
R^2	0.9978	R^2	0.9581

Table 3
Literature pertaining the adsorption of MB dye onto various adsorbents.

Dye	Adsorbent	pH	q_e	Ref
Methylene blue	Ulva Lactuca marine algae	8	91 %	[47]
Methylene blue	Seaweed biomass	5		[48]
Methylene blue	Chromochloris zofingiensis	10	135.42 mg/g	[49]
Methylene blue	Anadara granosa	12	98.6 %	[50]
Methylene blue	Bambuseae	–	629 mg/g	[51]
Methylene blue	Cigaratte butts	8	285.7 mg/g	[52]
Methylene blue	Arenga pinnata shell	–	203.86 mg/g	[53]
Methylene blue	Banana peel ash		98.54 %	[54]
Methylene blue	Chitosan resin	11	28.8 mg/g	[55]
Methylene blue	Chitosan cross-linked corncob	12	499.8 mg/g	[56]
Methylene blue	Fig waste chitosan coated hydrogels	–	103.1 mg/g	[57]
Methylene blue	Tricholoma Matsutake (TMF)	6	59.42 ± 2.058 mg/g	This study
Methylene blue	Tricholoma Matsutake functionalized chitosan (TMFC)	8	160.25 ± 6.207 mg/g	This study

6.2. Adsorption kinetics

Solid-liquid equilibrium studies offer insights into the final state of an adsorption process but do not elucidate the reaction pathways or mechanisms for transferring solutes from the liquid phase to the solid surface. In contrast, establishing adsorption equilibrium clarifies the solute transfer mechanism across the two-phase boundary, influenced by the physicochemical properties of the solid sorbent and the solutes partitioning behavior, as indicated by the partitioning coefficient. To fully understand factors such as retention time, sorption rate, and potential rate-limiting steps, adsorption kinetic studies are essential [58]. The current research evaluates the adsorption mechanism of MB onto TMF and TMFC using established kinetic models: pseudo-first-order (PFO) and pseudo-second-order (PSO). These models, represented by specific non-linear Eqs. (5) and (6), facilitate the analysis of temperature dependence in sorption kinetics [59]. Kinetic data were analyzed by plotting equilibrium adsorption capacity (qe) versus time (t) at different temperature conditions for both models, as shown in Fig. 6 (a–f).

$$\text{PFO kinetics}: \; q_t = q_{e1}(1 - \exp(-k_1 t)) \tag{5}$$

$$\text{PSO kinetics}: \; q_t = \frac{q_{e2}^2 k_2 t}{1 + q_{e2} k_2 t} \tag{6}$$

where q_e, q_t are the amount of the dye adsorbed onto the surface of TMF, TMFC, t is equilibrium, k_1,k_2 are the rate constants for PSO and PFO respectively. Table 4 provides a comprehensive comparison of the adsorption parameters derived from both kinetic models, including equilibrium capacities, rate constants, and coefficients of determination (R^2). The coefficient of determination (R^2) for the adsorption of MB dye onto TMF and TMFC was found to be 0.99 for the PSO model, compared to 0.94 for the PFO model. The higher R^2 value for the PSO model than the PFO, and better fit of the experimental to the calculated data suggests the underlying adsorption mechanism of MB onto TMF, TMFC is predominantly governed by chemisorption. The chemisorption mechanism suggest that the formation of chemical bonds, rather than physical adsorption dictates the adsorption rate. Further, the chemisorption mechanism signifies a strong affinity between the adsorbent and the dye molecules, resulting in an effective capture mechanism.

In summary, the application of isotherm and kinetic models in this study reveals critical insights into the adsorption behavior of methylene blue onto TMFC. The Langmuir isotherm model exhibited the best fit, suggesting monolayer adsorption on a homogeneous surface with finite, well-defined binding sites, and a high adsorption capacity. Kinetic analysis, particularly the fit to the pseudo-second-order model, points to chemisorption as the primary mechanism, involving the sharing or

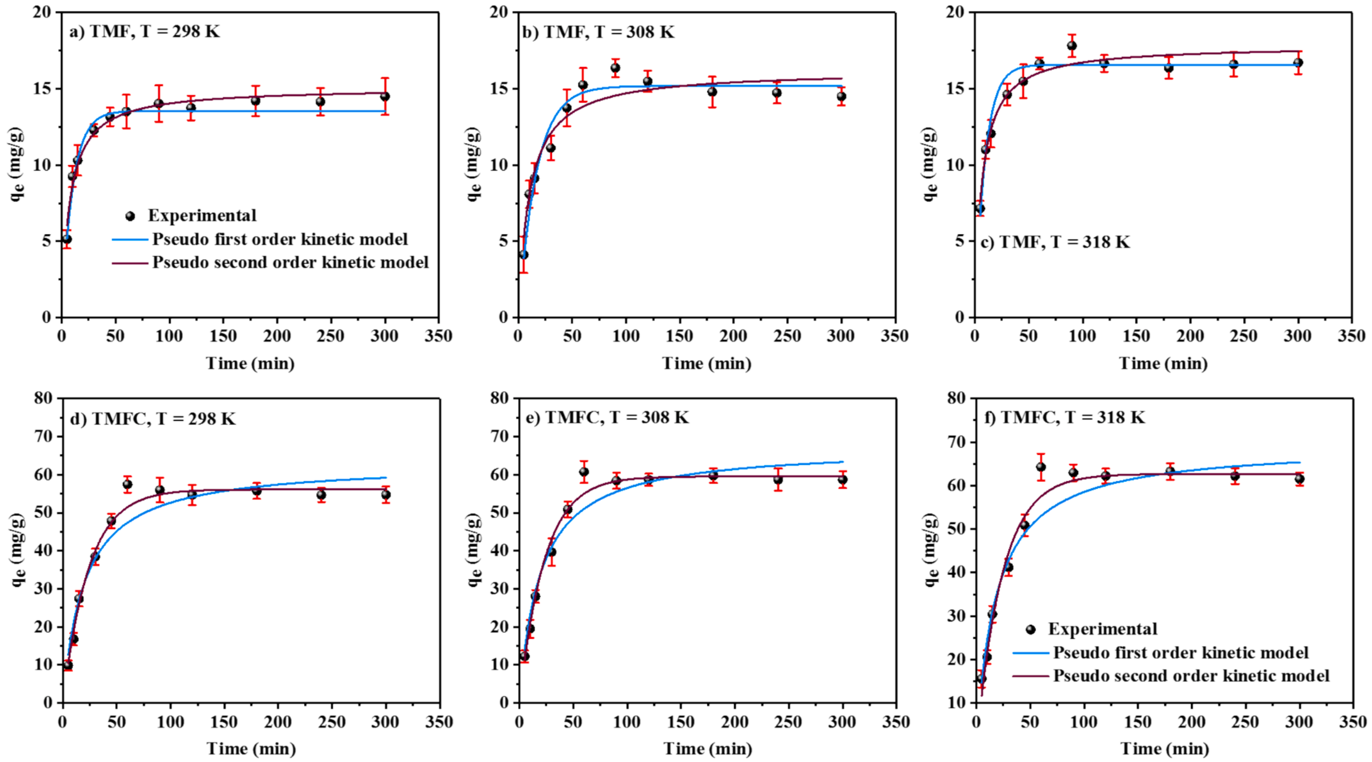

Fig. 6. Non-linear kinetic studies varied with temperature using adsorbents (a–c) TMF, (d–f) TMFC.

Table 4
Kinetic modeling data for the separation of MB dye using TMF, TMFC.

Sorbent		Pseudo first-order kinetic			Pseudo second-order kinetic		
	Temp (K)	$q_{e1\ (cal)}$ (mg/g)	k_1 (1/min)	R^2	$q_{e2\ (cal)}$ (mg/g)	K_2 (g/mg min)	R^2
a) *TMF*							
TMF	298	11.86 ± 0.177	0.095 ± 0.005	0.9126	14.91 ± 0.211	0.0094 ± 0.001	0.9958
	308	18.08 ± 0.338	0.061 ± 0.006	0.9429	20.38 ± 0.567	0.0055 ± 0.001	0.9918
	318	21.52 ± 0.265	0.098 ± 0.002	0.9587	26.64 ± 0.303	0.0088 ± 0.001	0.9927
b) *TMFC*							
TMFC	298	58.22 ± 0.769	0.036 ± 0.007	0.9253	59.37 ± 3.197	0.0007 ± 0.0001	0.9926
	308	67.85 ± 2.407	0.039 ± 0.004	0.9371	67.38 ± 2.407	0.0007 ± 0.0001	0.9919
	318	75.33 ± 2.201	0.001 ± 0.0001	0.9562	74.39 ± 2.325	0.0007 ± 0.001	0.9930

exchange of electrons between the dye molecules and the adsorbent's functional groups. These findings underscore the superior adsorption efficiency of the biomass adsorbent, offering a robust and predictable framework for optimizing dye removal in practical wastewater treatment scenarios.

6.3. *Adsorption thermodynamics*

Thermodynamic parameters such as Gibbs free energy, change in entropy, enthalpy variations defines the reaction nature, possibility of the adsorption mechanism, spontaneity, and nature of the inherent energetic changes. The knowledge on the influence of temperature is analyzed through ΔG^0, ΔH^0, ΔS^0, and equilibrium constants and the representative Eqs. (8)–(11) are listed below [60]. The slope of plot depicting 1/T vs (ln K_c) reveals the enthalpy change, while the entropy changes can be determined from the y-intercept of the same plot.

$$\Delta G^0 = -RT\ln K_c \tag{8}$$

$$K_c = \frac{C_{Ae}}{C_e} \tag{9}$$

$$\Delta G^0 = \Delta H^0 - T\Delta S^0 \tag{10}$$

$$\ln K_c = -\frac{\Delta G^0}{RT} = -\frac{\Delta H^0}{RT} + \frac{\Delta S^0}{R} \tag{11}$$

where the variables R, T, Kc, C_{Ae}, C_e, are known to be universal gas constant (J/mol. K), absolute temperature (K), distribution coefficient, equilibrium concentrations (mg/L) of MB on sorbent TMF, TMFC respectively.

The present batch adsorption studies were performed across a temperature range between 298–328 K, using 0.03 g of adsorbent TMF, and 0.02 g of TMFC per 300 mg/L of MB dye solution. The results presented in Fig. 7 demonstrated that the adsorption capacity for MB dyes increased with rising temperature, indicating that the adsorption process is endothermic in nature [61]. Further, the endothermic nature is also confirmed through the negative slope of the plot confirmed the endothermic nature, indicating that influence of temperature holds the key in adsorption mechanism.

Increased adsorption at higher temperatures indicates that added energy helps overcome the activation barrier, enhancing interactions

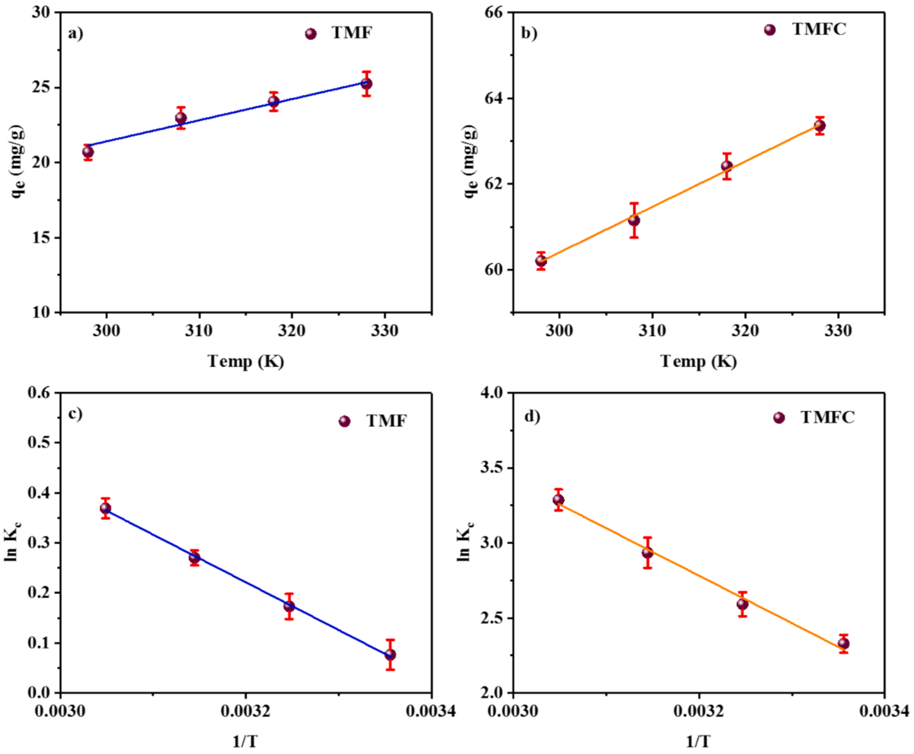

Fig. 7. (a and b) Effect of temperature on the adsorption of MB dye onto TMF, TMFC (c and d) van't Hoff plot for the adsorption of MB dye onto the TMF, TMFC.

between methylene blue (MB) molecules and the sorbent materials (TMF, TMFC). Elevated temperatures also alter the diffusion behavior of sorbate molecules, increasing the mass transfer rate from the bulk solution to the boundary layer around the sorbent surface.

Additionally, higher temperatures strengthen intermolecular forces between the adsorbate and adsorbent, facilitating greater mobility of sorbate molecules toward the sorbent surface. The detailed summary of these thermodynamic aspects were presented in Table 5. From the Table the positive ΔH°value signifies endothermic nature of the adsorption phenomenon, while the ΔS°value reflects the increase in randomness at the solid–liquid interface during the adsorption [62], and the negative ΔG°values further confirm the spontaneous nature of the adsorption process. In summary, the temperature effects on MB dye adsorption onto TMF, TMFC contribute to a deeper understanding of the thermodynamic aspects of dye adsorption, which is crucial for optimizing adsorption conditions in practical applications.

7. Adsorption mechanism

The adsorption mechanism of MB dye molecule onto TMFC involves several interaction pathways (see Fig. 8). TMFC sorbent, known for its intrinsic porosity, serves as a baseline for evaluating the enhancements brought about by chitosan functionalization. Chitosan contains abundant amine (–NH_2) and hydroxyl (–OH) groups, which can protonate under acidic conditions, leading to increased electrostatic attraction with the anionic sites of the MB molecules.

Table 5
Thermodynamic assessment on adsorption of MB dye onto TMFand TMFC.

Temp (K)	ΔG^0 (kJ/mol)	ΔH^0 (kJ/mol)	ΔS^0 (J/ mol K)
(a) TMF			
298	−0.189	7.92	28.97
308	−0.443		
318	−0.714		
328	−1.006		
(b) TMFC			
298	−5.914	24.60	108.58
308	−6.634		
318	−7.756		
328	−8.959		

FTIR studies confirms the successful functionalization of chitosan into the biomass evident by the appearance of the new peak at 1325 cm^{-1} denoting the C–N stretching vibrations, peaks at 1021 cm^{-1} (C–O stretching) and 1156 cm^{-1} (asymmetric C–O–C stretching in the glucosamine ring), indicating intact polysaccharide structures. While, broad bands in the range of 3200–3500 cm^{-1} reflect overlapping O–H and N–H stretching vibrations, confirming the presence of hydroxyl and amino groups that enhance adsorption through hydrogen bonding [63]. Further, the functionalization of chitosan onto biomass significantly alters the biomass surface properties, enhancing its adsorption capabilities. Point of zero charge (PZC) analysis reveals a notable shift in the biomass surface charge after chitosan functionalization. The PZC decreases possibly due to deprotonation of functional groups of biomass increasing the negative surface charge density. This shift improves the biomass interaction with cationic MB molecules [64]. pH dependent adsorption studies further elucidate the optimal conditions for MB removal, demonstrating that the highest adsorption capacity is achieved at basic pH. At higher pH values, the biomass surface maintains a predominantly negative charge, promoting favorable electrostatic interactions with the positively charged MB with the increasing pH. Hence, the adsorption of dye can be elucidated by two interaction modes, primarily electrostatic attraction between the positively charged atoms on MB and the negatively charged carbonyl and oxygen atoms on the chitosan-functionalized biomass (see Fig. 8). Secondly, conceivable interaction that further anchors the dye to the biomass surface is the formation of hydrogen bonding between nitrogen atoms of MB dye which can act as hydrogen-bond acceptors and OH groups of chitosan and biomass that can act as hydrogen-bond donors [65]. This dual mechanism of electrostatic, and hydrogen bonding interactions underpins the substantial improvement in adsorption capacity of biomass. The functionalization process not only increases the surface area of the

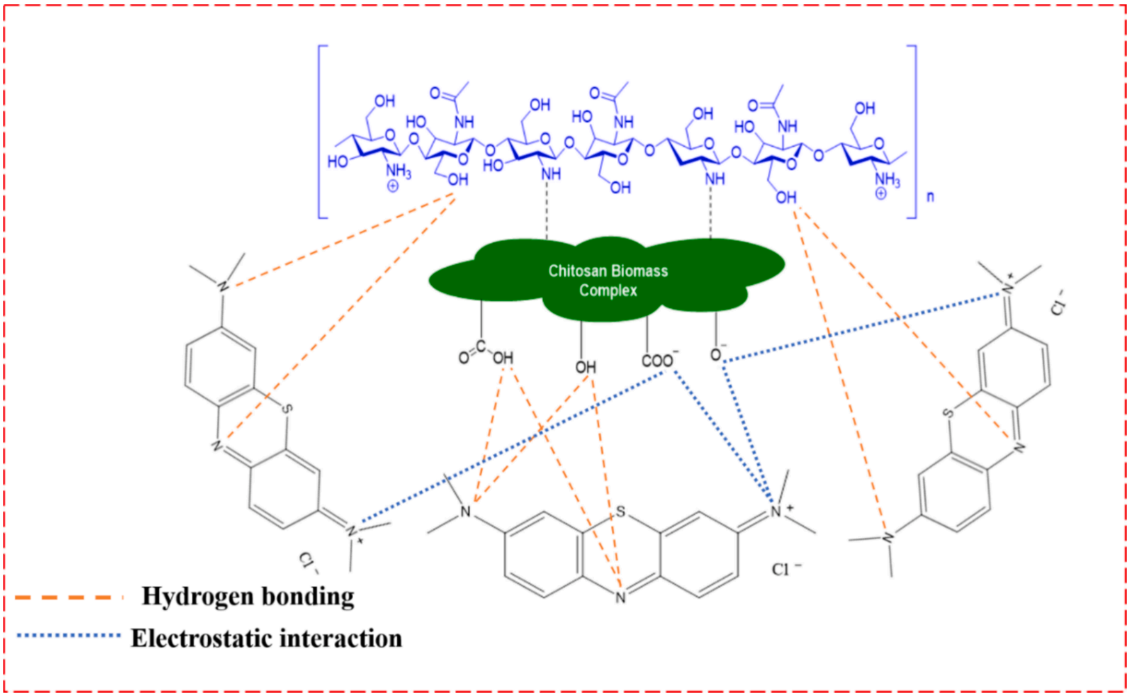

Fig. 8. Demonstration of plausible interactions involved in adsorption mechanism of MB dye on TMFC.

biomass but also optimizes its structural configuration, leading to enhanced accessibility and efficiency as a sorbent material. This comprehensive analysis underscores the synergistic effects of chitosan modification, which enhances both the electrostatic and hydrogen bonding interactions, leading to superior MB dye molecule removal performance. Consequently, TMFC emerges as a highly efficient material for environmental remediation applications, providing valuable insights into optimizing biomass-based adsorbents.

8. Desorption and recycling studies

8.1. Desorption of adsorbent

Scaling up adsorption processes for real-world water treatment applications necessitates a deep understanding of the reusability and regeneration capabilities of the selected adsorbents. This study explores into the regeneration properties of TMF, TMFC through meticulous sorption–desorption cycles (see Fig. 9a). To do, separate experiments were conducted using 30 mL of 300 ppm MB dye solution. Varying dosages were utilized for TMF (0.03 g), TMFC (0.02 g) were added to 300 mg/L MB dye solutions to ensure optimal contact between the adsorbent and the target dye molecules. The solution pH was precisely maintained at the optimal values of pH 6 (TMF) and pH 8 (TMFC). These specific pH conditions promote favorable interactions between the adsorbent surface and the MB dye molecules [66]. The experiments were conducted at room temperature (298 K) to mimic real-world operating conditions. Additionally, controlled agitation speeds were applied: 200 rpm (TMF) and 300 rpm for (TMFC), agitation time 90 min (TMF) and 60 min (TMFC) were applied to ensure sufficient dosage, contact time for effective adsorption.

After the adsorption process, the solutions were dried in a furnace at 333 K for 8 h to remove any residual water. The resulting solid residue (sediment) was then meticulously recovered for subsequent desorption studies. Further, to identify the most effective medium for recovering the spent adsorbents, a diverse range of eluents were investigated. These include acidic solution 0.1 N HCl to explore potential ion-exchange mechanisms, alkaline solution 0.1 N NaOH to probe interactions with surface functional groups, and organic solvents 100 % C_2H_5OH to assess their potential for desorption [67]. Among the selected eluents, HCl showed the better desorption capacity, indicating MB, being a cationic dye, binds to the negatively charged functional groups on the adsorbent surface through electrostatic attraction. Acidic solutions like HCl provide an abundance of H^+ ions, which compete with the positively charged MB molecules for binding sites, effectively breaking the electrostatic interactions and facilitating dye desorption. The use of 0.1 N concentration balances effectiveness and material stability, avoiding excessive acid strength that could damage the adsorbent structure. Additionally, HCl is widely available, cost-effective, and easy to handle,

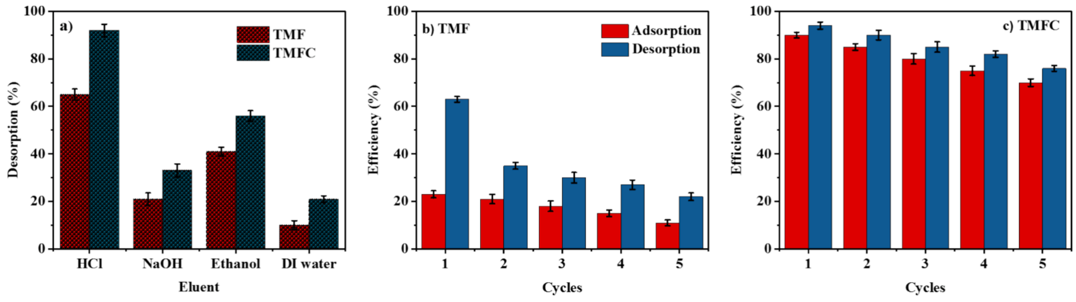

Fig. 9. Desorption of adsorbent from solutions (a) MB dye onto TMF, TMFC, (b) adsorption–desorption cycle of TMF, (c) adsorption–desorption cycle of TMFC.

making it a practical choice for sustainable and efficient adsorbent regeneration. This study successfully evaluates the reusability of TMF, TMFC for MB dye molecules removal. The identified optimal eluents offer promising avenues for developing cost-effective and sustainable water treatment processes. Furthermore, these findings pave the way for future research on optimizing regeneration cycles and minimizing eluent consumption. By minimizing eluent usage and exploring environmentally friendly regeneration strategies, a truly sustainable and environmentally friendly approach to metal remediation can be established.

8.2. Recycling studies

While the initial potential of TMF and TMFC as reusable adsorbents for Mb dye molecule is evident, a closer look at their regeneration efficiency tested via multiple adsorption–desorption cycles, reveals the real challenges. This study probes into this crucial aspect, exploring the effect of these adsorbents fare over repeated use. The critical findings involves, for MB dye molecule removal, TMF exhibited a sharp decline in efficiency after just two cycles with a drop of adsorption efficiency from 22 %–15 %, while desorption efficiency also decreased significantly from 62 %–28 % respectively (see Fig. 9b). This suggests that MB removal weakens considerably after the second regeneration cycle, rendering the TMF adsorbent less suitable for long-term MB dye remediation applications. However, a more optimistic scenario emerges for MB dye removal with TMFC sorbent material. Here, TMFC demonstrates remarkable resilience, maintaining acceptable adsorption efficiency between 80–86 % even after five consecutive cycles. Desorption efficiency also remains decent, balanced above 75 % (see Fig. 9c) [68]. These findings suggest that TMFC could be viable option over TMF for MB dye molecule remediation in settings requiring multiple treatment cycles. This highlights the importance of evaluating reusability across different target pollutants to gain a comprehensive understanding of an adsorbents true capabilities.

9. Conclusion

This research successfully developed and thoroughly characterized a novel chitosan-functionalized Tricholoma matsutake adsorbent for the removal of methylene blue (MB) dye from aqueous solutions. The functionalized biomass (TMFC) exhibited high adsorption efficiency, with isotherm model analyses confirming its superior capacity for dye molecule removal. Kinetic studies indicated that the adsorption process follows a pseudo-second order model, suggesting chemisorption as the dominant mechanism. Thermodynamic assessments revealed that the adsorption is both endothermic and spontaneous. Regeneration studies demonstrated excellent reusability, with the TMFC adsorbent maintaining significant adsorption efficiency over five consecutive adsorption–desorption cycles, outperforming conventional adsorbents in both performance and cost-effectiveness. The environmentally benign nature of the functionalized adsorbent, derived from sustainable biomass and modified with polymer compounds, underscores its potential as an eco-friendly and efficient solution for dye removal from contaminated water.

CRediT authorship contribution statement

Anjani R.K. Gollakota: Writing – original draft, Methodology, Formal analysis, Conceptualization. **Munagapati Venkata Subbaiah:** Writing – review & editing, Formal analysis. **Arshdeep Singh:** Conceptualization, Validation. **Chi-Min Shu:** Supervision, Conceptualization, Writing – review & editing, Resources. **Prakash Kumar Sarangi:** Data curation, Conceptualization. **Jet-Chau Wen:** Supervision, Writing – review & editing.

Declaration of competing interest

The authors declare that they have no known competing financial interests or personal relationships that could have appeared to influence the work reported in this paper.

Acknowledgements

The authors sincerely appreciate the efforts and timely support of PS&DPL group.

Data availability

Data will be made available on request.

References

[1] I. Khan, K. Saeed, I. Zekker, B. Zhang, A. Hendi, A. Ahmad, S. Ahmad, N. Zada, H. Ahmad, L. Ali Shah, T. Shah, I. Khan, Review on methylene blue: its properties, uses, toxicity and photodegradation, Water 14 (2022) 1–30, https://doi.org/10.5040/9781501365072.12105.

[2] B.M. Adesanmi, Y.-T. Hung, H. Paul, C. Huhnke, Comparison of dye wastewater treatment methods: a review. Comparison of dye wastewater treatment methods: a review, GSC Adv. Res. Rev. 10 (2022) 126–137, https://doi.org/10.5281/zenodo.6331586.

[3] N. ElMessaoudi, Y. Miyah, Z.M. Şenol, Z. Ciğeroğlu, E.S. Kazan-Kaya, S. Gubernat, J. Georgin, D.S.P. Franco, Comprehensive analytical review of heavy metal removal efficiency using agricultural solid waste-based bionanocomposites, Nano-Struct. Nano-Objects 38 (2024), https://doi.org/10.1016/j.nanoso.2024.101220.

[4] N. ElMessaoudi, Y. Miyah, M. Benjelloun, J. Georgin, D.S.P. Franco, Z.M. Şenol, Z. Ciğeroğlu, M. ElHajam, S. Knani, P. Nguyen-Tri, A comprehensive review on designing nanocomposite adsorbents for efficient removal of 4-nitrophenol from water, Nano-Struct. Nano-Objects 40 (2024), https://doi.org/10.1016/j.nanoso.2024.101326.

[5] N. ElMessaoudi, Y. Miyah, J. Georgin, M. Wasilewska, R.J.A. Felisardo, H. Moukadiri, M.S. Manzar, A.A. Aryee, S. Knani, M.M. Rahman, Recent developments in the synthesis of tetraethylenepentamine-based nanocomposites to eliminate heavy metal pollutants from wastewater through adsorption, Bioresour. Technol. Rep. 28 (2024), https://doi.org/10.1016/j.biteb.2024.101982.

[6] J. Georgin, D.S.P. Franco, Y. Dehmani, P. Nguyen-Tri, N. ElMessaoudi, Current status of advancement in remediation technologies for the toxic metal mercury in the environment: a critical review, Sci. Total Environ. 947 (2024) 174501, https://doi.org/10.1016/j.scitotenv.2024.174501.

[7] E. Kurtulbaş, Z. Ciğeroğlu, S. Şahin, N. ElMessaoudi, V. Mehmeti, Monte Carlo, molecular dynamic, and experimental studies of the removal of malachite green using g-C3N4/ZnO/Chitosan nanocomposite in the presence of a deep eutectic solvent, Int. J. Biol. Macromol. 274 (2024), https://doi.org/10.1016/j.ijbiomac.2024.133378.

[8] Y. Miyah, N. ElMessaoudi, M. Benjelloun, J. Georgin, D.S.P. Franco, Y. Acikbas, H. S. Kusuma, M. Sillanpää, MOF-derived magnetic nanocomposites as potential formulations for the efficient removal of organic pollutants from water via adsorption and advanced oxidation processes: a review, Mater. Today Sustain. 28 (2024), https://doi.org/10.1016/j.mtsust.2024.100985.

[9] A. Holilah, N. ElMessaoudi, M. Ulfa, A. Hamzah, Z.A.A. Hamid, D.V. Ramadhani, L. Suryanegara, M. Mahardika, A.T. Melenia, A.W. Pratama, D. Prasetyoko, Fabrication a sustainable adsorbent nanocellulose-mesoporous hectorite bead for methylene blue adsorption, Case Stud. Chem. Environ. Eng. 10 (2024) 100850, https://doi.org/10.1016/j.cscee.2024.100850.

[10] S. Fatullayeva, D. Tagiyev, N. Zeynalov, S. Mammadova, E. Aliyeva, Recent advances of chitosan-based polymers in biomedical applications and environmental protection, J. Polym. Res. 29 (2022), https://doi.org/10.1007/s10965-022-03121-3.

[11] F. Ahmadi, Z. Oveisi, M. Samani, Z. Amoozgar, Chitosan based hydrogels: characteristics and pharmaceutical applications, Res. Pharm. Sci. 10 (2015) 1–16.

[12] A. Lesbani, N. Ahmad, R. Mohadi, I. Royani, S. Wibiyan, Y.H. Amri, Selective adsorption of cationic dyes by layered double hydroxide with assist algae (Spirulina platensis) to enrich functional groups, JCIS Open 15 (2024) 100118, https://doi.org/10.1016/j.jciso.2024.100118.

[13] S. Suleman Ismail Abdalla, H. Katas, J.Y. Chan, P. Ganasan, F. Azmi, M. Fauzi Mh Busra, Antimicrobial activity of multifaceted lactoferrin or graphene oxide functionalized silver nanocomposites biosynthesized using mushroom waste and chitosan, RSC Adv. 10 (2020) 4969–4983, https://doi.org/10.1039/c9ra08680c.

[14] M. Rinaudo, G. Pavlov, J. Desbrieres, Influence of acetic acid concentration on the solubilization of chitosan, Int. J. Polym. Polym. (Guildf). 40 (1999) 7029–7032.

[15] K.S.W. Sing, D.H. Everett, R.A.W. Haul, L. Moscou, R.A. Pierotti, J. Rouquerol, T. Siemieniewska, Reporting physisorption data for gas/solid systems with special reference to the determination of surface area and porosity, Pure Appl. Chem. 57 (1985) 603–619, https://doi.org/10.1351/pac198557040603.

[16] E.P. Barrett, L.G. Joyner, P.P. Halenda, The determination of pore volume and area distributions in porous substances. I. Computations from nitrogen isotherms, J. Am. Chem. Soc. 73 (1951) 373–380, https://doi.org/10.1021/ja01145a126.

[17] A. Venault, L. Vachoud, C. Pochat, D. Bouyer, C. Faur, Elaboration of chitosan/activated carbon composites for the removal of organic micropollutants from waters, Environ. Technol. 29 (2008) 1285–1296, https://doi.org/10.1080/09593330802296256.

[18] B. Zhong, L. Zhang, J. Yu, K. Fan, Ultrafine iron-cobalt nanoparticles embedded in nitrogen-doped porous carbon matrix for oxygen reduction reaction and zinc-air batteries, J. Colloid Interface Sci. 546 (2019) 113–121, https://doi.org/10.1016/j.jcis.2019.03.038.

[19] H. Li, E.C. Minor, P.K. Zigah, Diagenetic changes in Lake Superior sediments as seen from FTIR and 2D correlation spectroscopy, Org. Geochem. 58 (2013) 125–136, https://doi.org/10.1016/j.orggeochem.2013.03.002.

[20] C. Kundu, S. Biswas, B.S. Thomas, D. Appadoo, A. Duan, S. Bhattacharya, Evolution of functional group of lignocellulosic biomass and its delignified form during thermal conversion using synchrotron-based THz and laboratory-based in-situ DRIFT spectroscopy, Fuel 348 (2023) 128579, https://doi.org/10.1016/j.fuel.2023.128579.

[21] R. Varma, S. Vasudevan, S. Chelladurai, A. Narayanasamy, Synthesis and physicochemical characteristics of chitosan extracted from pinna deltoides, Lett. Appl. Nanobiosci. 11 (2021) 4061–4070, https://doi.org/10.33263/lianbs114.40614070.

[22] R. Labied, O. Benturki, A.Y. Eddine Hamitouche, A. Donnot, Adsorption of hexavalent chromium by activated carbon obtained from a waste lignocellulosic material (Ziziphus jujuba cores): kinetic, equilibrium, and thermodynamic study, Adsorpt. Sci. Technol. 36 (2018) 1066–1099, https://doi.org/10.1177/0263617417750739.

[23] A.S. Chatterley, P. Laity, C. Holland, T. Weidner, S. Woutersen, G. Giubertoni, Broadband multidimensional spectroscopy identifies the amide II vibrations in silkworm films, Molecules 27 (2022), https://doi.org/10.3390/molecules27196275.

[24] D.L. Setyaningrum, S. Riyanto, A. Rohman, Analysis of corn and soybean oils in red fruit oil using FTIR spectroscopy in combination with partial least square, Int. Food Res. J. 20 (2013) 1977–1981.

[25] A. Difusa, K. Mohanty, V.V. Goud, The chemometric approach applied to FTIR spectral data for the analysis of lipid content in microalgae cultivated in different nitrogen sources, Biomass Convers. Biorefinery. 6 (2016) 427–433, https://doi.org/10.1007/s13399-016-0198-6.

[26] O.Y. Abdelaziz, C.P. Hulteberg, Physicochemical characterisation of technical lignins for their potential valorisation, Waste Biomass Valoriz. 8 (2017) 859–869, https://doi.org/10.1007/s12649-016-9643-9.

[27] A. Arafat, S. Samad, S. Masum, Preparation and characterization of chitosan from shrimp shell waste, Int. J. Sci. Eng. Res. 6 (2015) 538–541. https://www.researchgate.net/profile/Sabrin-Samad/publication/282641814_Preparation_and_Characterization_of_Chitosan_from_Shrimp_shell_waste/links/5614cd6808aed47facee936c/Preparation-and-Characterization-of-Chitosan-from-Shrimp-shell-waste.pdf.

[28] M.S. Bostan, E.C. Mutlu, H. Kazak, S. Sinan Keskin, E.T. Oner, M.S. Eroglu, Comprehensive characterization of chitosan/PEO/levan ternary blend films, Carbohydr. Polym. 102 (2014) 993–1000, https://doi.org/10.1016/j.carbpol.2013.09.096.

[29] A. OU, I. Bo, Chitosan hydrogels and their glutaraldehyde-crosslinked counterparts as potential drug release and tissue engineering systems – synthesis, characterization, swelling kinetics and mechanism, J. Phys. Chem. Biophys. 07 (2017), https://doi.org/10.4172/2161-0398.1000256.

[30] M.F. Queiroz, K.R.T. Melo, D.A. Sabry, G.L. Sassaki, H.A.O. Rocha, Does the use of chitosan contribute to oxalate kidney stone formation? Mar. Drugs. 13 (2015) 141–158, https://doi.org/10.3390/md13010141.

[31] N.B. Duong, C.L. Wang, L.Z. Huang, W.T. Fang, H. Yang, Development of a facile and low-cost chitosan-modified carbon cloth for efficient self-pumping enzymatic biofuel cells, J. Power Sources. 429 (2019) 111–119, https://doi.org/10.1016/j.jpowsour.2019.05.001.

[32] B.W. Chieng, N.A. Ibrahim, W.M.Z.W. Yunus, M.Z. Hussein, Poly(lactic acid)/poly(ethylene glycol) polymer nanocomposites: Effects of graphene nanoplatelets, Polymers (Basel). 6 (2014) 93–104, https://doi.org/10.3390/polym6010093.

[33] A. Nanditha, J. Manokaran, N. Balasubramanian, Fabrication of Lys-PVA-Fe3O4 modified electrode for the electrochemical determination of uric acid, Res. J. Chem. Environ. 18 (2014) 54–61.

[34] A. Kasprzhitskii, G. Lazorenko, A. Kruglikov, I. Kuchkina, V. Gorodov, Effect of silane functionalization on properties of poly(Lactic acid)/palygorskite nanocomposites, Inorganics. 9 (2021) 1–11, https://doi.org/10.3390/inorganics9010003.

[35] J.M. Tan, S. Bullo, S. Fakurazi, M.Z. Hussein, Characterization of betulinic acid-multiwalled carbon nanotubes modified with hydrophilic biopolymer for improved biocompatibility on nih/3t3 cell line, Polymers (Basel) 13 (2021), https://doi.org/10.3390/polym13091362.

[36] L. Ceroni, S. Benazzato, S. Pressi, L. Calvillo, E. Marotta, E. Menna, Enhanced adsorption of methylene blue dye on functionalized multi-walled carbon nanotubes, Nanomaterials 14 (2024), https://doi.org/10.3390/nano14060522.

[37] A. Putra, S. Fauzia, D. Deswati, S. Arief, R. Zein, The potential of duck egg white as a modifier for activated rice straw to enhance Cr(VI) ions adsorption in an aqueous solution, South African, J. Chem. Eng. 48 (2024) 204–213, https://doi.org/10.1016/j.sajce:2024.02.002.

[38] D. Yan, Y. Li, Y. Liu, N. Li, X. Zhang, C. Yan, Antimicrobial properties of chitosan and chitosan derivatives in the treatment of enteric infections, Molecules 26 (2021), https://doi.org/10.3390/molecules26237136.

[39] C. Daniele, S. Alves, B. Healy, L.A.D.A. Pinto, T.R. Sant, A. Cadaval, C.B. Breslin, Recent Developments in Chitosan-Based Adsorbents for the Removal of Pollutants from Aqueous Environments, 2021.

[40] A. Gollakota, V. Munagapati, S. Liao, C. Shu, K. Shadangi, P. Sarangi, J. Wen, Ionic liquid [bmim] [TFSI] templated Na-X zeolite for the adsorption of (Cd2+, Zn2+), and dyes (AR, R6), Environ. Res. 216 (2023) 114525.

[41] Y. Liu, Y. Zheng, A. Wang, Enhanced adsorption of Methylene Blue from aqueous solution by chitosan-g-poly (acrylic acid)/vermiculite hydrogel composites, J. Environ. Sci. 22 (2010) 486–493, https://doi.org/10.1016/S1001-0742(09)60134-0.

[42] R.A. Shawabkeh, M.F. Tutunji, Experimental study and modeling of basic dye sorption by diatomaceous clay, Appl. Clay Sci. 24 (2003) 111–120, https://doi.org/10.1016/S0169-1317(03)00154-6.

[43] M.A. Al-Ghouti, M.A.M. Khraisheh, M.N.M. Ahmad, S. Allen, Adsorption behaviour of methylene blue onto Jordanian diatomite: a kinetic study, J. Hazard. Mater. 165 (2009) 589–598, https://doi.org/10.1016/j.jhazmat.2008.10.018.

[44] L.Y. Jun, N.M. Mubarak, M.J. Yee, L.S. Yon, C.H. Bing, M. Khalid, E.C. Abdullah, An overview of functionalised carbon nanomaterial for organic pollutant removal, J. Ind. Eng. Chem. 67 (2018) 175–186, https://doi.org/10.1016/j.jiec.2018.06.028.

[45] I. Langmuir, The adsorption of gases on plane surfaces of glass, mica and platinum, Eucken, Verh. Deut. Phys. Ges. 16 (1918) 1361–1403, https://doi.org/10.1021/ja01269a066.

[46] V.H.Freundlich, Kolloidfiillung und Adsorption., Juretzka Gattierung von Zinkblende Und Galmei. 20 (1907) 750–754. doi:10.1002/ange.19070201806.

[47] D. Pratiwi, D.J. Prasetyo, C.D. Poeloengasih, Adsorption of Methylene Blue dye using Marine algae Ulva lactuca, IOP Conf. Ser. Earth Environ. Sci. 251 (2019), https://doi.org/10.1088/1755-1315/251/1/012012.

[48] D. Jiang, H. Li, X. Cheng, Q. Ling, H. Chen, B. Barati, Q. Yao, A. Abomohra, X. Hu, P. Bartocci, S. Wang, A mechanism study of methylene blue adsorption on seaweed biomass derived carbon: from macroscopic to microscopic scale, Process Saf. Environ. Prot. 172 (2023) 1132–1143, https://doi.org/10.1016/j.psep.2023.02.044.

[49] M. Bayat, E. Salehi, M. Mahdieh, Chromochloris zofingiensis microalgae as a potential dye adsorbent: adsorption thermo-kinetic, isothermal, and process optimization, Algal Res. 71 (2023) 103043, https://doi.org/10.1016/j.algal.2023.103043.

[50] M. Valussi, M. Antonelli, D. Donelli, F. Firenzuoli, Jo l P of, Perspect. Med. (2021) 100451, https://doi.org/10.1016/j.rineng.2024.102715.

[51] J. Alchouron, A.L. Bursztyn Fuentes, C. Guerreiro, K. Hodara, M.N. Gatti, C. U. Pittman, T.E. Mlsna, H.D. Chludil, A.S. Vega, The feedstock anatomical properties determine biochar adsorption capacities: a study using woody bamboos (Bambuseae) and methylene blue as a model molecule, Chemosphere 362 (2024) 142656, https://doi.org/10.1016/j.chemosphere.2024.142656.

[52] A. Dalmaz, S. Sivrikaya özak, Methylene blue dye efficient removal using activated carbon developed from waste cigarette butts: adsorption, thermodynamic and kinetics, Fuel 372 (2024), https://doi.org/10.1016/j.fuel.2024.132151.

[53] M. Mariana, E.M. Mistar, T. Alfatah, Functional properties and continuous adsorption process of Arenga pinnata shell and its porous biochars for aqueous methylene blue removal, Mater. Chem. Phys. 322 (2024) 129484, https://doi.org/10.1016/j.matchemphys.2024.129484.

[54] A. Sarkar, N. Mushahary, B. Das, S. Basumatary, A novel approach for modification of montmorillonite using banana peel ash extract for enhanced adsorption efficiency of methylene blue dye, Desalin. Water Treat. 320 (2024) 100585, https://doi.org/10.1016/j.dwt.2024.100585.

[55] J. Xue, W. Mao, Y. Wang, J. Li, M. Wu, Preparation of spherical chitosan resin and adsorption of methylene blue, Rare Met. 30 (2011) 249–253, https://doi.org/10.1007/s12598-011-0279-4.

[56] X.J. Liu, M.F. Li, J.F. Ma, J. Bian, F. Peng, Chitosan crosslinked composite based on corncob lignin biochar to adsorb methylene blue: kinetics, isotherm, and thermodynamics, Colloids Surf. A Physicochem. Eng. Asp. 642 (2022) 128621, https://doi.org/10.1016/j.colsurfa.2022.128621.

[57] A. Parlayici, S. Aras, Chitosan coated biomass waste-based magnetic hydrogel beads for the removal of methylene blue, Int. J. Phytoremed. 26 (2024) 1500–1517.

[58] K.Y. Foo, B.H. Hameed, Insights into the modeling of adsorption isotherm systems, Chem. Eng. J. 156 (2010) 2–10, https://doi.org/10.1016/j.cej.2009.09.013.

[59] Y.S. Ho, G. McKay, Pseudo-second order model for sorption processes, Process Biochem. 34 (1999) 451–465, https://doi.org/10.1021/acs.oprd.7b00090.

[60] A. ElJery, H.S.K. Alawamleh, M.H. Sami, H.A. Abbas, S.S. Sammen, A. Ahsan, M. A. Imteaz, A. Shanableh, M. Shafiquzzaman, H. Osman, N. Al-Ansari, Isotherms, kinetics and thermodynamic mechanism of methylene blue dye adsorption on synthesized activated carbon, Sci. Rep. 14 (2024) 1–12, https://doi.org/10.1038/s41598-023-50937-0.

[61] A.R.K. Gollakota, V. Subbaiah Munagapati, C.M. Shu, J.C. Wen, Adsorption of Cr (VI), and Pb (II) from aqueous solution by 1-Butyl-3-methylimidazolium bis (trifluoromethylsulfonyl)imide functionalized biomass Hazel Sterculia (Sterculia Foetida L.), J. Mol. Liq. 350 (2022) 118534, https://doi.org/10.1016/j.molliq.2022.118534.

[62] M. Maruthapandi, V.B. Kumar, J.H.T. Luong, A. Gedanken, Kinetics, isotherm, and thermodynamic studies of methylene blue adsorption on polyaniline and polypyrrole macro-nanoparticles synthesized by C-dot-initiated polymerization, ACS Omega 3 (2018) 7196–7203, https://doi.org/10.1021/acsomega.8b00478.

[63] M.S. Rostami, M.M. Khodaei, Chitosan-based composite films to remove cationic and anionic dyes simultaneously from aqueous solutions: modeling and optimization using RSM, Int. J. Biol. Macromol. 235 (2023) 123723, https://doi.org/10.1016/j.ijbiomac.2023.123723.

[64] A. Kausar, K. Naeem, M. Tariq, Z.I.H. Nazli, H.N. Bhatti, F. Jubeen, A. Nazir, M. Iqbal, Preparation and characterization of chitosan/clay composite for direct

Rose FRN dye removal from aqueous media: comparison of linear and non-linear regression methods, J. Mater. Res. Technol. 8 (2019) 1161–1174, https://doi.org/10.1016/j.jmrt.2018.07.020.

[65] N.H. Azeman, N. Arsad, A.A.A. Bakar, Polysaccharides as the sensing material for metal ion detection-based optical sensor applications, Sensors (Switzerland). 20 (2020) 1–22, https://doi.org/10.3390/s20143924.

[66] S. Babel, T.A. Kurniawan, Low-cost adsorbents for heavy metals uptake from contaminated water: a review, J. Hazard. Mater. 97 (2003) 219–243, https://doi.org/10.1016/S0304-3894(02)00263-7.

[67] Momina, S. Mohammad, I. Suzylawati, Study of the adsorption/desorption of MB dye solution using bentonite adsorbent coating, J. Water Process Eng. 34 (2020), https://doi.org/10.1016/j.jwpe.2020.101155.

[68] K. Chauhan, P. Singh, K. Sen, R.K. Singhal, V.K. Thakur, Recent advancements in the field of chitosan/cellulose-based nanocomposites for maximizing arsenic removal from aqueous environment, ACS Omega 9 (2024) 27766–27788, https://doi.org/10.1021/acsomega.3c09713.